# The Effect of the Tetraalkylammonium Cation in the Electrochemical $CO_2$ Reduction Reaction on Copper Electrode


Connor Deacon-Price[1], Louis Changeur[1], Cássia S. Santana[1,§], Amanda C. Garcia[1,*]

*Van't Hoff Institute for Molecular Sciences, University of Amsterdam, Science Park 904, 1098 XH, Amsterdam, The Netherlands*

(*) Corresponding author: a.c.garcia@uva.nl

(§) Current address: HTC 31, Holst Centre / TNO &IMEC-nl, High Tech Campus 31, 5656AE, The Netherlands.


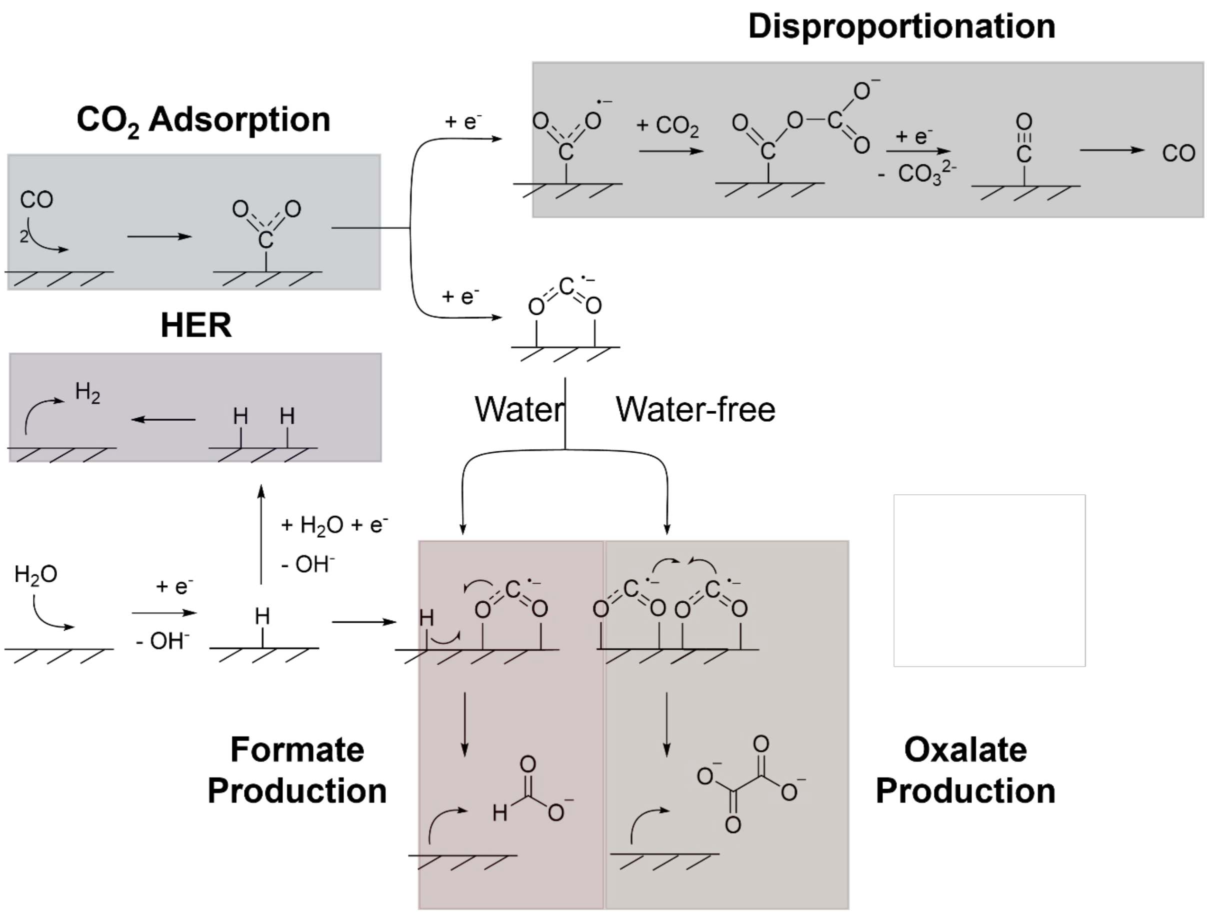


**Scheme S1**. A proposed mechanism for the formation of CO and $CO_3^{2-}$ through disproportionation (grey box), formate through protonation (red box), oxalate through radical recombination and dimerization (orange box), and hydrogen through HER (purple box) within a $CO_2$ adsorption-based regime.

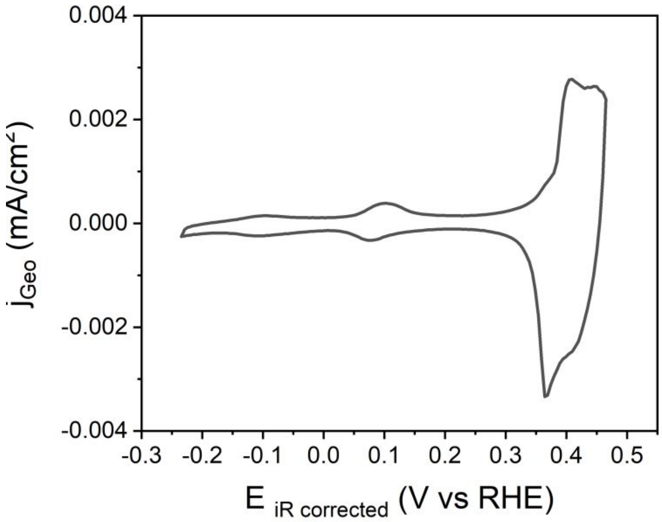


**Figure S1.** Cyclic voltammogram (CV) of polycrystalline Cu ($Cu_{Poly}$) in 0.1 M NaOH, under an Ar atmosphere, at a scan rate of 50 mV/s. CE = $Pt_{Poly}$; RE = RHE.

**Table S1** Table representing the water content in ppm, recorded by Karl-Fischer Titration, of each measured electrolyte condition when using dry MeCN.

| Salt | Concentration (M) | $H_2O$ content in Ar (ppm) | $H_2O$ content in $CO_2$ (ppm) |
|---|---|---|---|
| TEATFB | 0.05 | 21.0 | 21.0 |
| TEATFB | 0.10 | 25.4 | 25.4 |
| TEATFB | 0.50 | 25.8 | 25.8 |
| TEATFB | 0.75 | 31.1 | 31.1 |
| TPATFB | 0.05 | 19.0 | 16.3 |
| TPATFB | 0.10 | 18.2 | 14.3 |
| TPATFB | 0.50 | 4.0 | 23.1 |
| TPATFB | 0.75 | 7.4 | 18.8 |
| TBATFB | 0.05 | 16.0 | 17.2 |
| TBATFB | 0.10 | 12.4 | 12.8 |
| TBATFB | 0.50 | 17.4 | 21.3 |
| TBATFB | 0.75 | 17.1 | 17.1 |

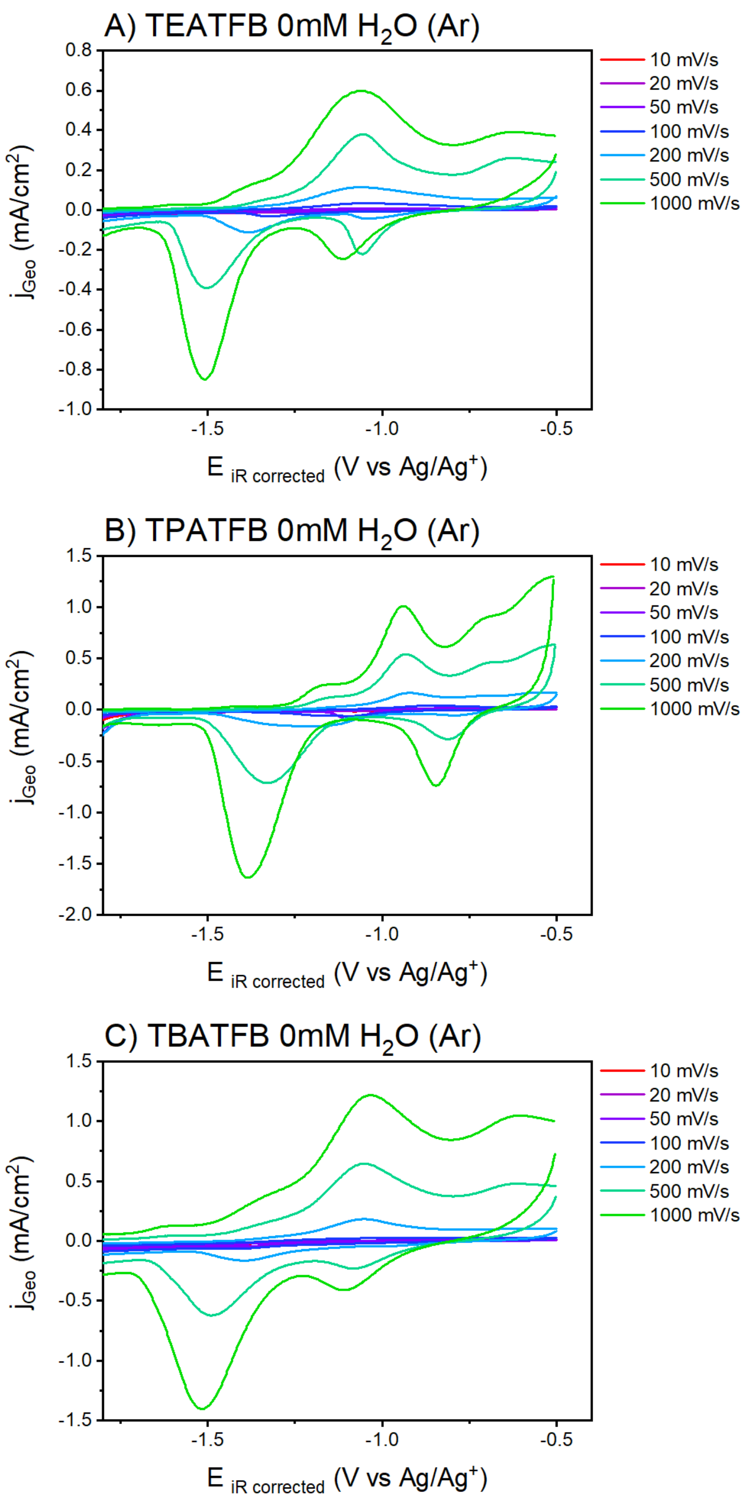


**Figure S2.** Cyclic Voltammograms of the CuPoly electrode, in A) 0.10 M TEATFB, B) 0.10 M TPATFB, and C) 0.10 M TBATFB in Ar deaerated conditions at various scan rates (10, 20, 50, 100, 200, 500, 1000 mV/s). CE = graphite, RE = commercial leak-free $Ag/Ag^{+}$

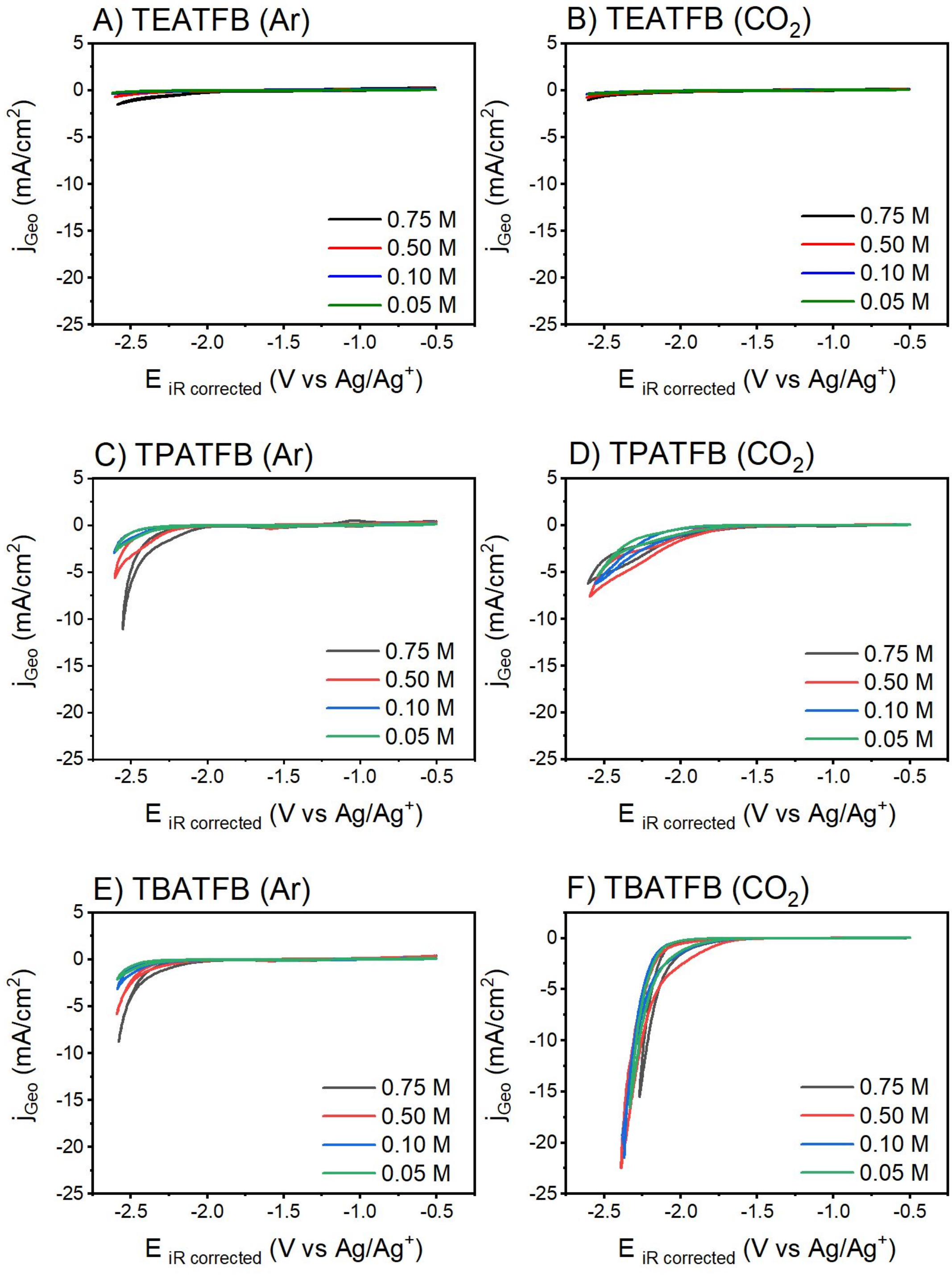


**Figure S3.** Cyclic Voltammetry (CVs) of $Cu_{poly}$ electrode, varying concentrations of TAAX salts in dry MeCN: A) TEATFB solution deaerated with Ar; B) $CO_2$ saturated TEATFB solution; C) TPATFB solution deaerated with Ar; D) $CO_2$ saturated TPATFB solution; E) TBATFB solution deaerated with Ar; F) $CO_2$ saturated TBATFB solution, at a scan rate of 50 mV/s.

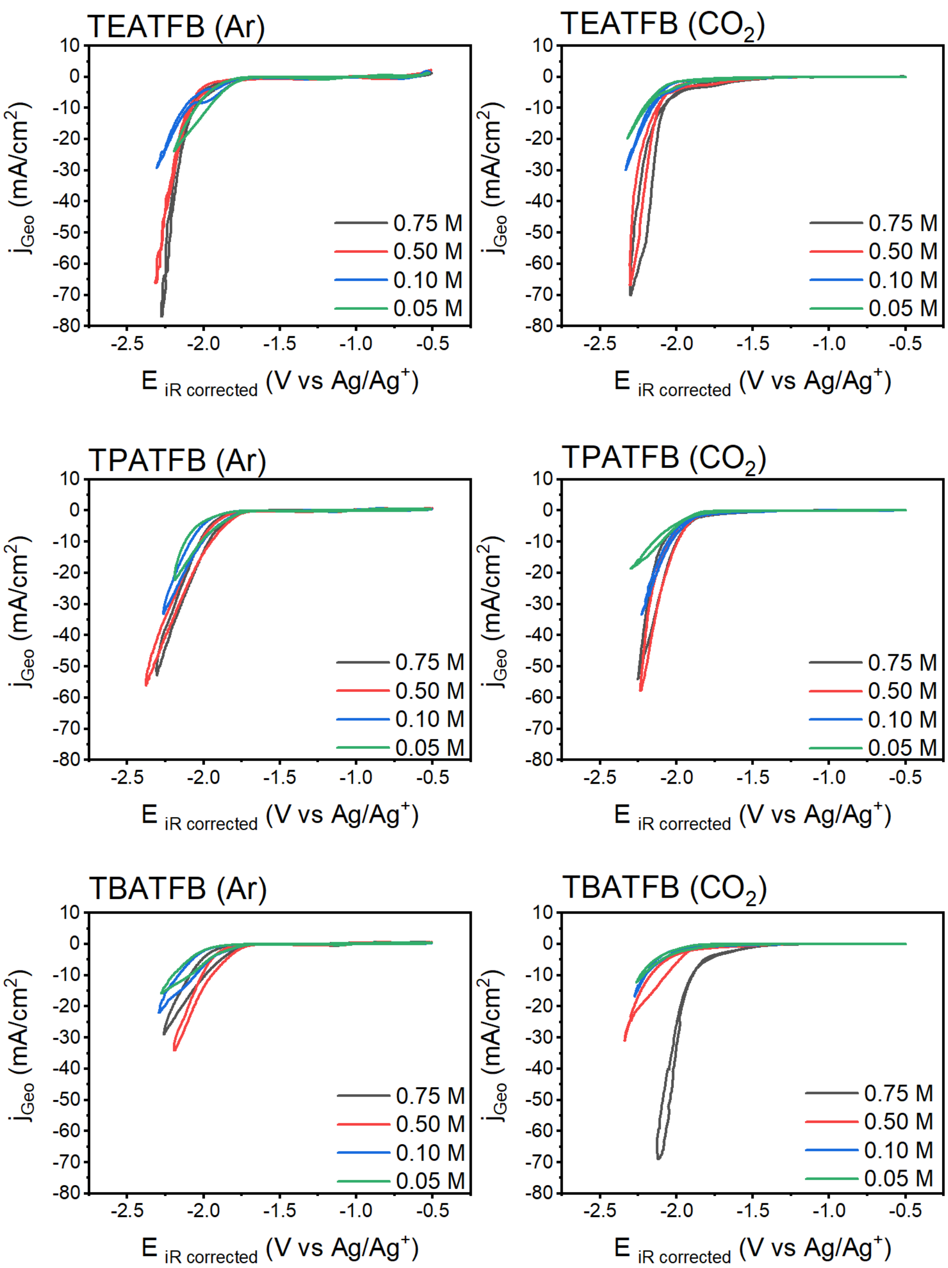


**Figure S4.** Cyclic Voltammetry (CVs) of $Cu_{poly}$ electrode, varying concentrations of TAAX salts in wet MeCN (1000 mM $H_2O$ addition): A) TEATFB solution deaerated with Ar; B) $CO_2$ saturated TEATFB solution; C) TPATFB solution deaerated with Ar; D) $CO_2$ saturated TPATFB solution; E) TBATFB solution deaerated with Ar; F) $CO_2$ saturated TBATFB solution, at a scan rate of 50 mV/s.

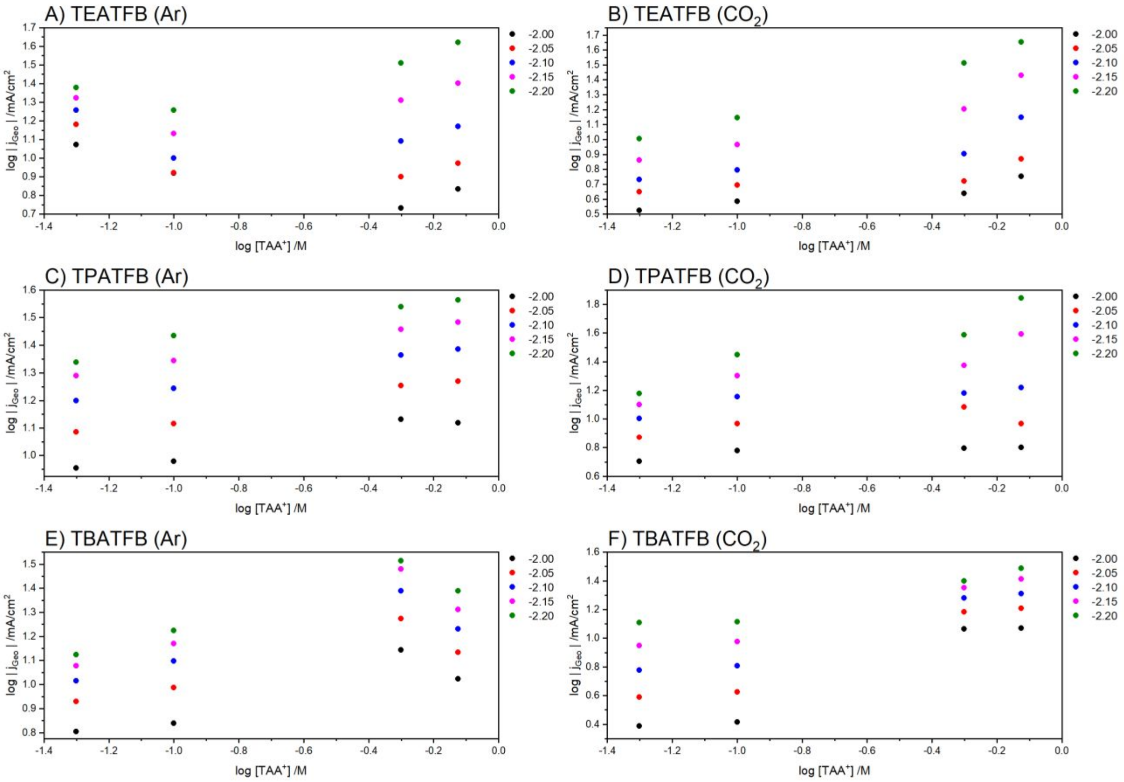


**Figure S5.** Reaction orders derived from cyclic voltammetry (CVs) of $Cu_{poly}$ electrode, varying concentrations of TAAX salts in wet MeCN (1000 mM $H_2O$ addition): A) TEATFB solution deaerated with Ar; B) $CO_2$ saturated TEATFB solution; C) TPATFB solution deaerated with Ar; D) $CO_2$ saturated TPATFB solution; E) TBATFB solution deaerated with Ar; F) $CO_2$ saturated TBATFB solution, at a scan rate of 50 mV/s.

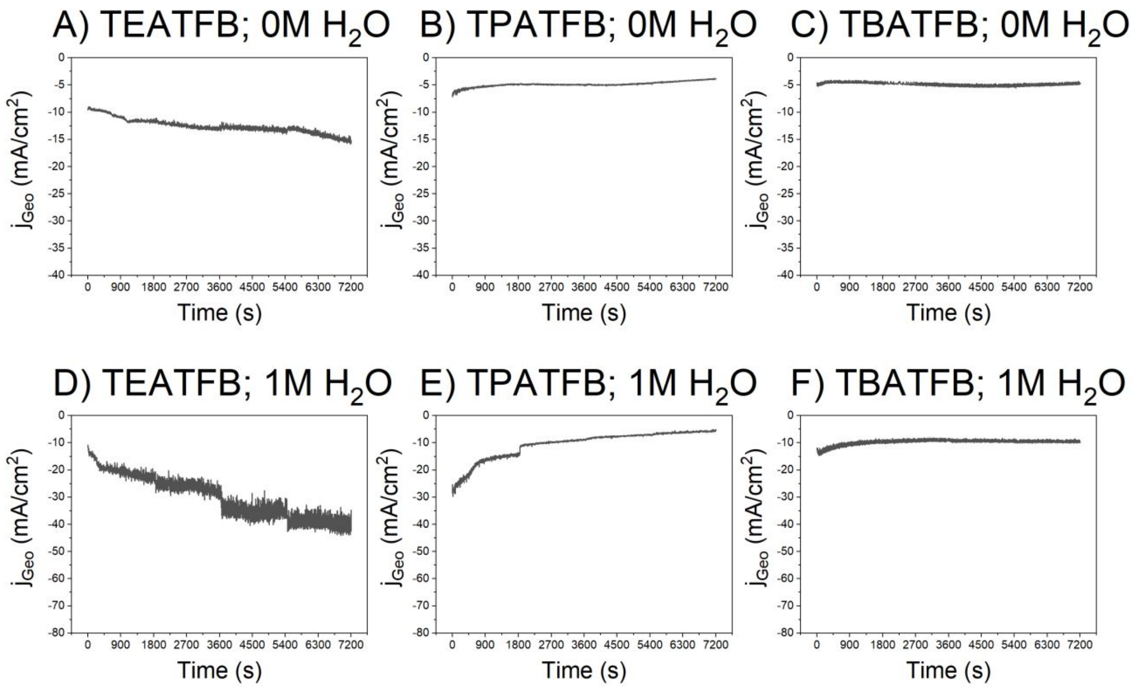


Figure S6. Chronoamperometry of $Cu_{poly}$ electrode in dry $CO_2$ saturated MeCN solutions using supporting electrolytes A) 0.05 M TEATFB, B) 0.05 M TPATFB, and C) 0.05 M TBATFB and $CO_2$ saturated MeCN solutions with 1M water, using supporting electrolytes D) 0.05 M TEATFB, E) 0.05 M TPATFB, and F) 0.05 M TBATFB.

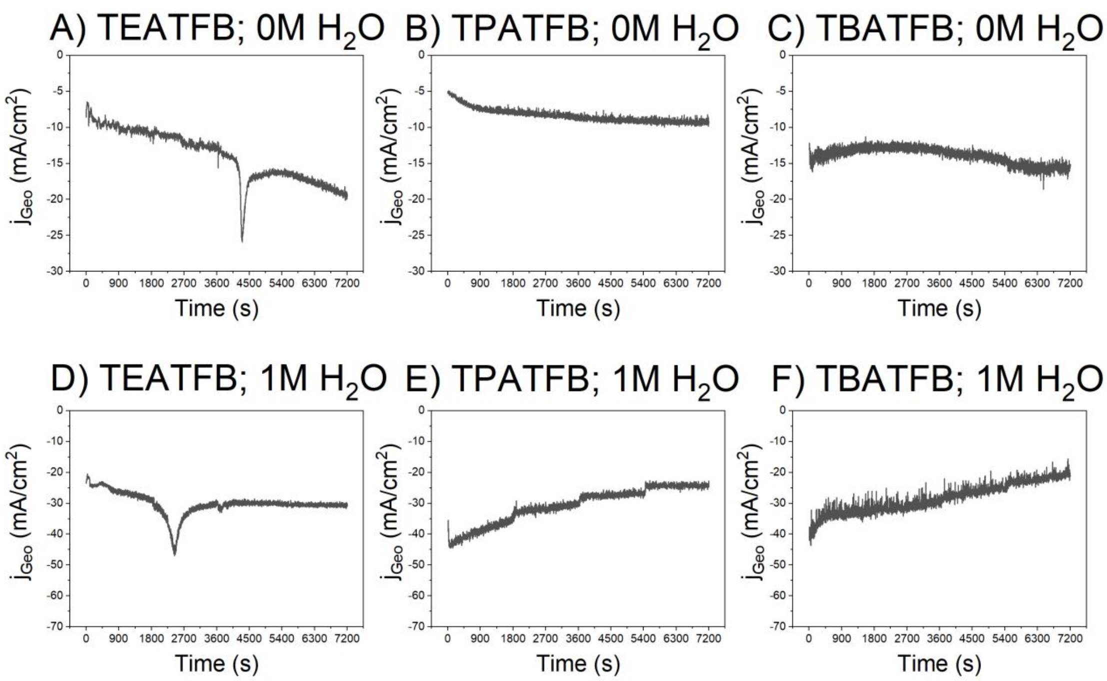


Figure S7. Chronoamperometry of $Cu_{poly}$ electrode in dry $CO_2$ saturated MeCN solutions using supporting electrolytes A) 0.75 M TEATFB, B) 0.75 M TPATFB, and C) 0.75 M TBATFB and $CO_2$ saturated MeCN solutions with 1M water, using supporting electrolytes D) 0.75 M TEATFB, E) 0.75 M TPATFB, and F) 0.75 M TBATFB.

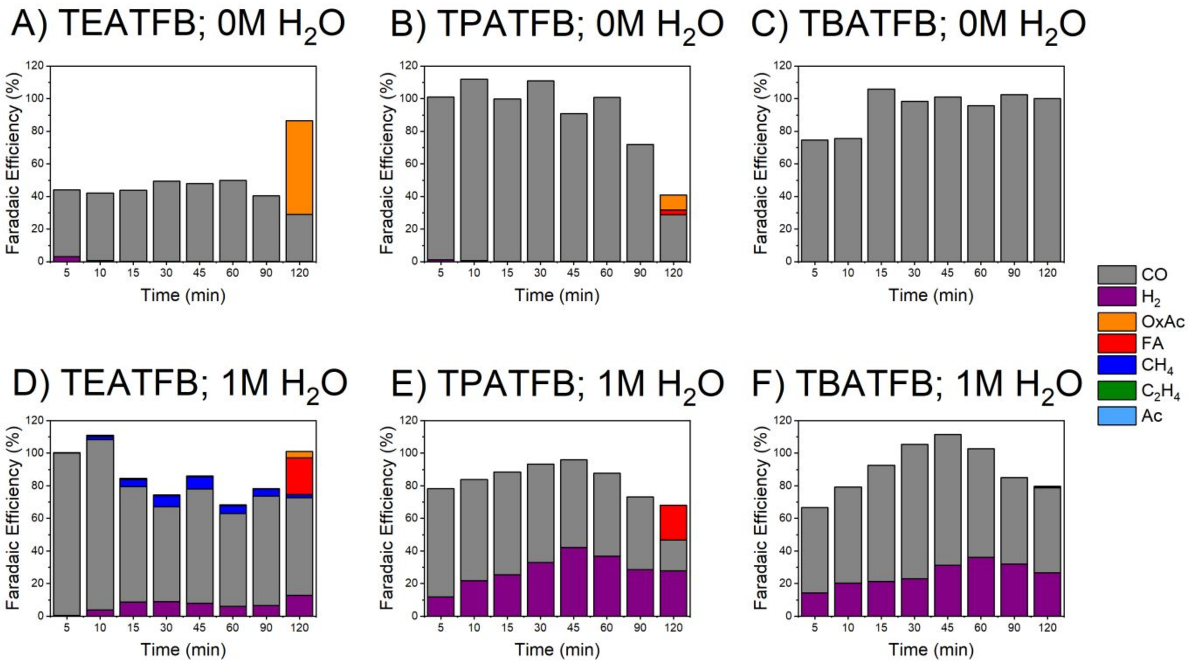


Figure S8. Time resolved Faradaic efficiencies (FE%) of $Cu_{poly}$ electrode in dry $CO_2$ saturated MeCN solutions using supporting electrolytes A) 0.05 M TEATFB, B) 0.05 M TPATFB, and C) 0.05 M TBATFB and $CO_2$ saturated MeCN solutions with 1M water, using supporting electrolytes D) 0.05 M TEATFB, E) 0.05 M TPATFB, and F) 0.05 M TBATFB. FE% was determined by online gas chromatography coupled with HPLC at -2.4 V vs. Ag/Ag+ for dry conditions, and at -2.1 V vs. Ag/Ag+ for wet conditions. Chronoamperometry was performed for a total of 120 min. Products are defined as follows: OA - oxalic acid; Ac - acetic acid; FA - formic acid; $C_2H_4$ - ethylene; $CH_4$ - methane; CO - carbon monoxide; $H_2$ - hydrogen.

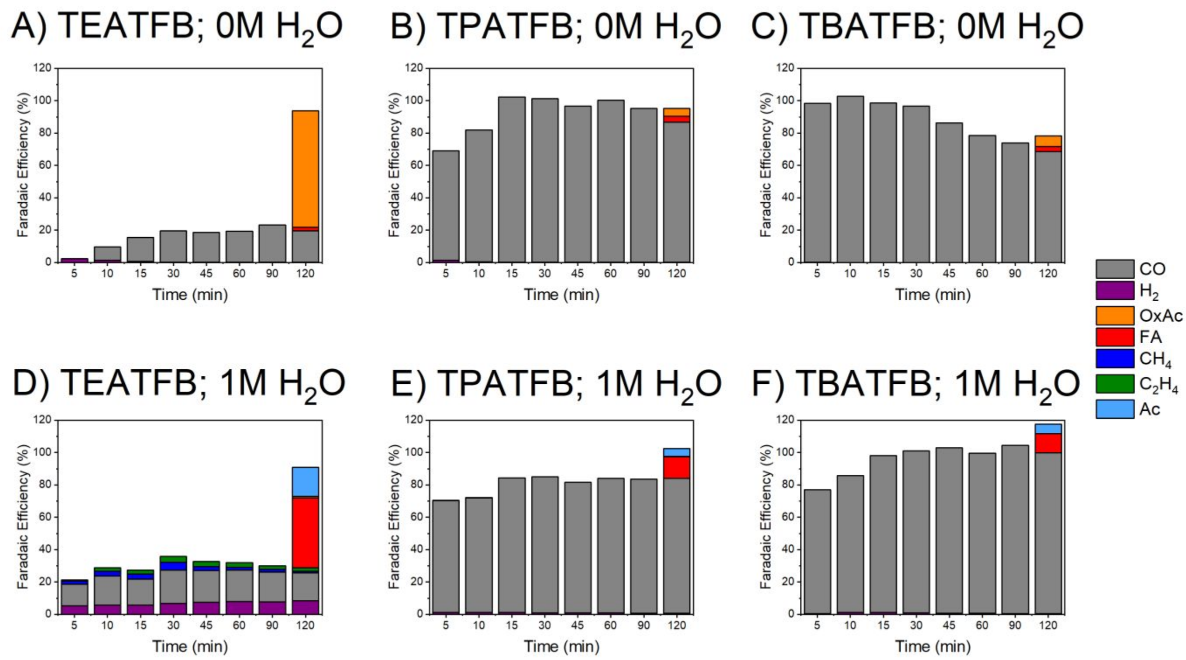

Figure S9. Time resolved Faradaic efficiencies (FE%) of $Cu_{poly}$ electrode in dry $CO_2$ saturated MeCN solutions using supporting electrolytes A) 0.75 M TEATFB, B) 0.75 M TPATFB, and C) 0.75 M TBATFB and $CO_2$ saturated MeCN solutions with 1M water, using supporting electrolytes D) 0.75 M TEATFB, E) 0.75 M TPATFB, and F) 0.75 M TBATFB. FE% was determined by online gas chromatography coupled with HPLC at -2.4 V vs. Ag/Ag+ for dry conditions, and at -2.1 V vs. Ag/Ag+ for wet conditions. Chronoamperometry was performed for a total of 120 min. Products are defined as follows: OA - oxalic acid; Ac - acetic acid; FA - formic acid; $C_2H_4$ - ethylene; $CH_4$ - methane; CO - carbon monoxide; $H_2$ - hydrogen.

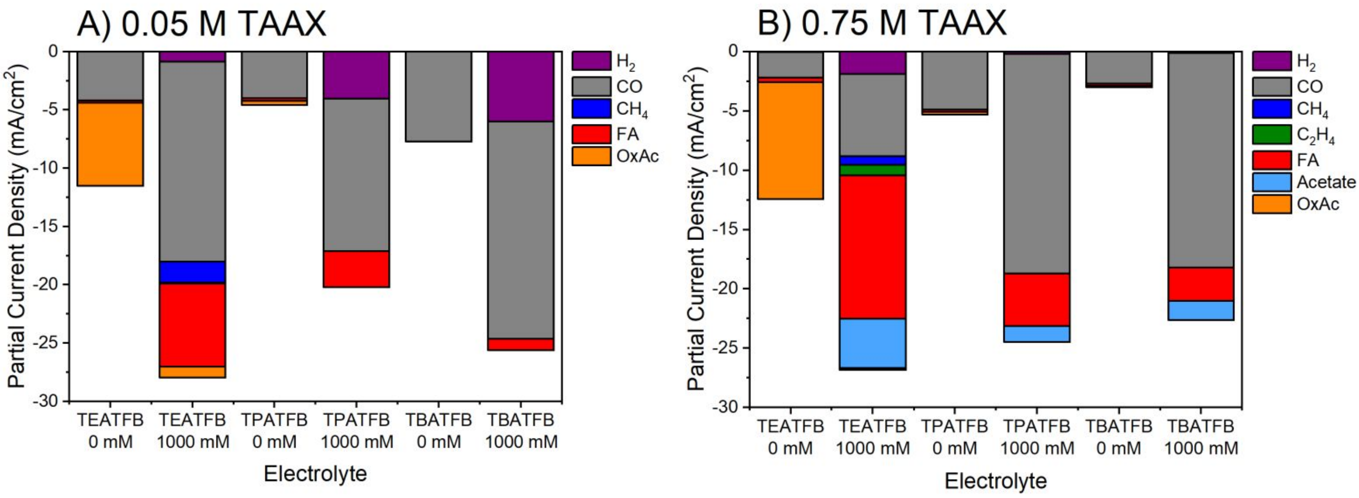


Figure S10. Partial current densities of $Cu_{poly}$ electrode, 0.05 M TAAX (A) and 0.75 M TAAX (B) in both dry and wet MeCN. For each salt, dry conditions are displayed on the left, and wet conditions are displayed on the right. Chronoamperometry was performed for a total of 120 min. Products are defined as follows: OA - oxalic acid; Ac - acetic acid; FA - formic acid; $C_2H_4$ - ethylene; $CH_4$ - methane; CO - carbon monoxide; $H_2$ - hydrogen.

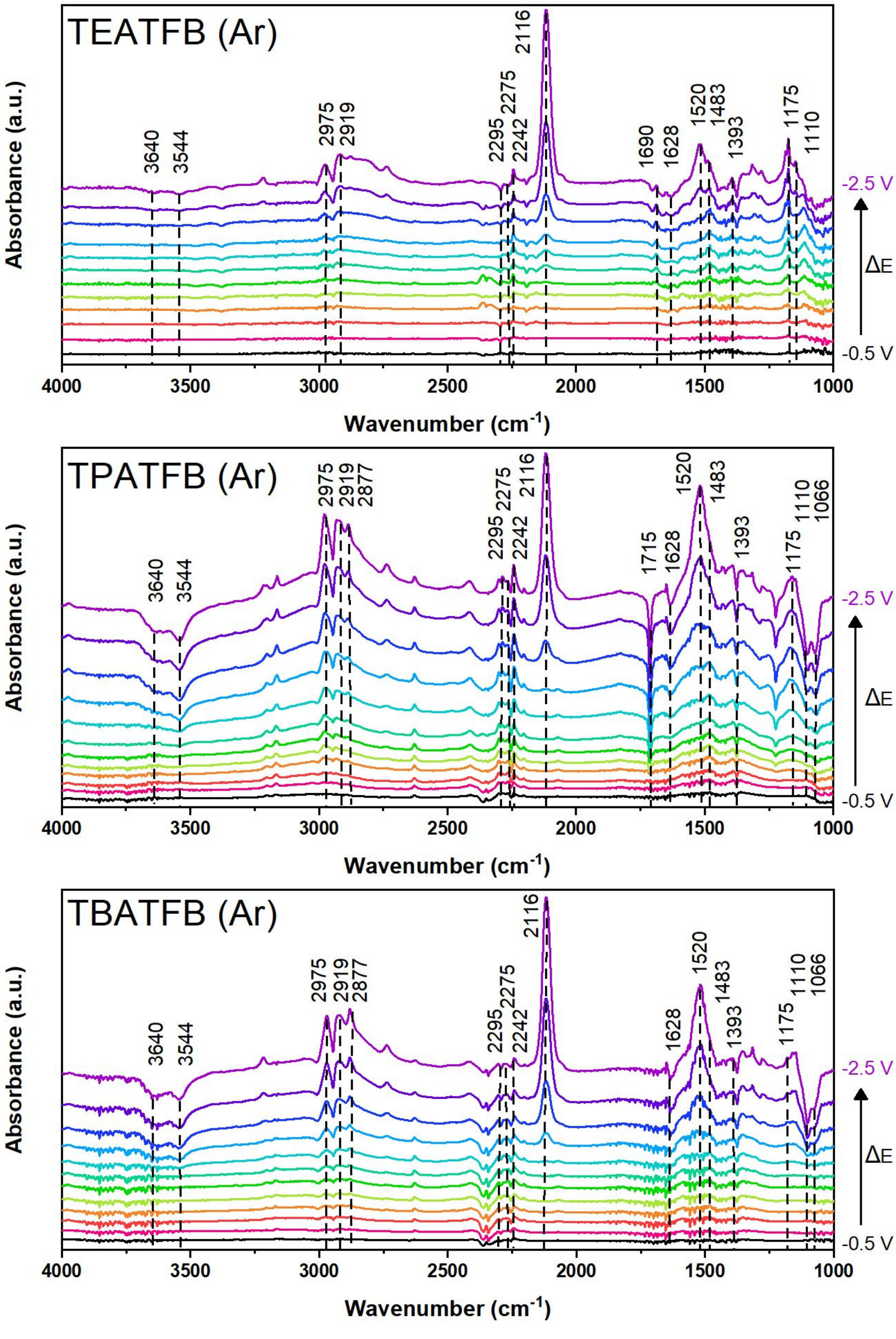


**Figure S11.** Electrochemical *in situ* FTIR spectra for dry 0.05 M TEATFB, TPATFB, and TBATFB MeCN electrolytes, in Ar deaerated conditions, at $Cu_{Poly}$ WE. Background signals are recorded at -0.5 V vs $Ag/Ag^+$. Spectra are recorded at -0.5 V, then -1.0 V, increasing by -200 mV until -2.0 V, then increasing by -100 mV until -2.5 V.

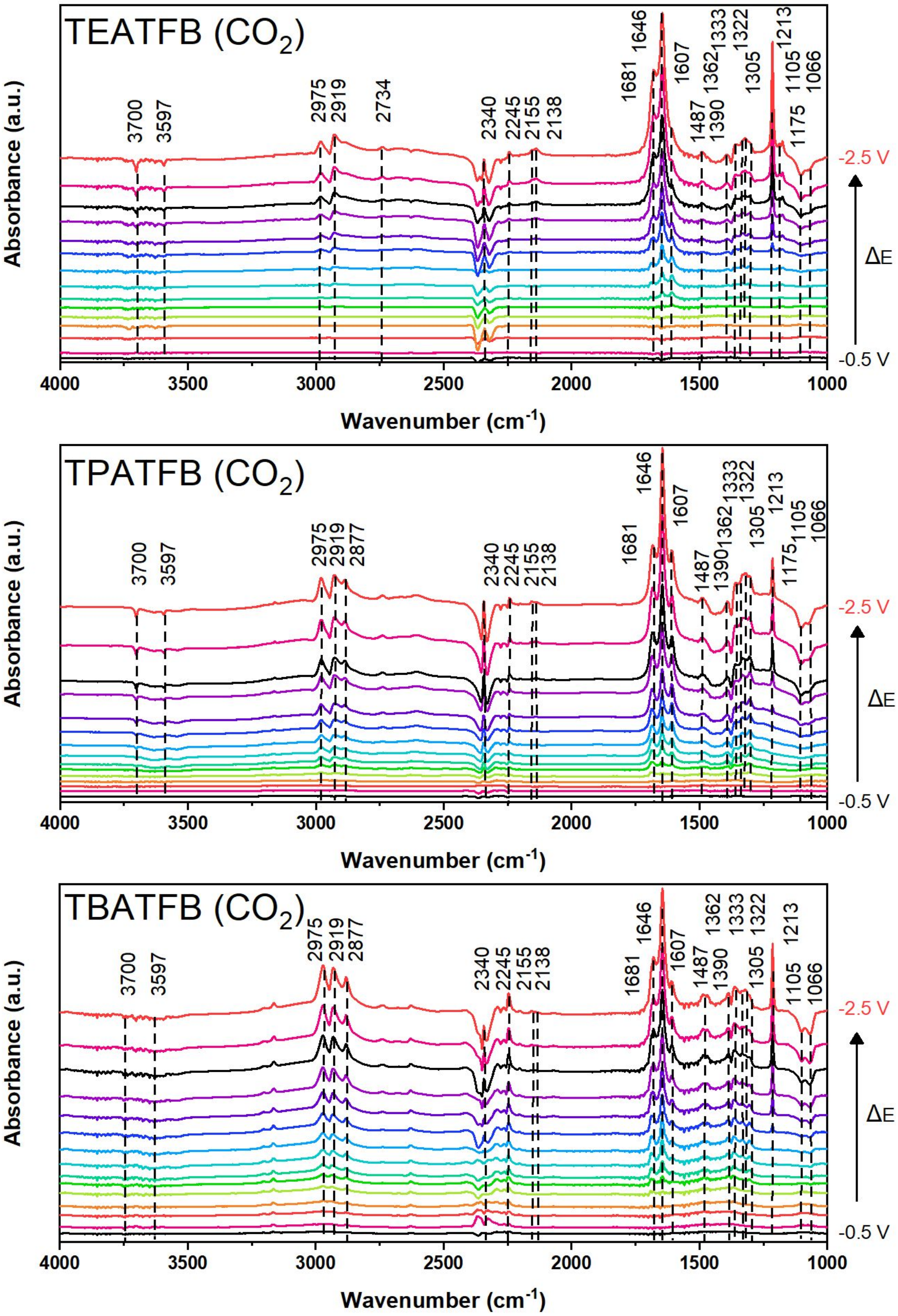


**Figure S12.** Electrochemical *in situ* FTIR spectra for dry 0.05 M TEATFB, TPATFB, and TBATFB MeCN electrolytes in $CO_2$ saturated conditions, at $Cu_{Poly}$ WE. Background signals are recorded at -0.5 V vs $Ag/Ag^+$. Spectra are recorded at -0.5 V, then -1.0 V, increasing by -200 mV until -1.4 V, then increasing by -100 mV until -2.5 V.

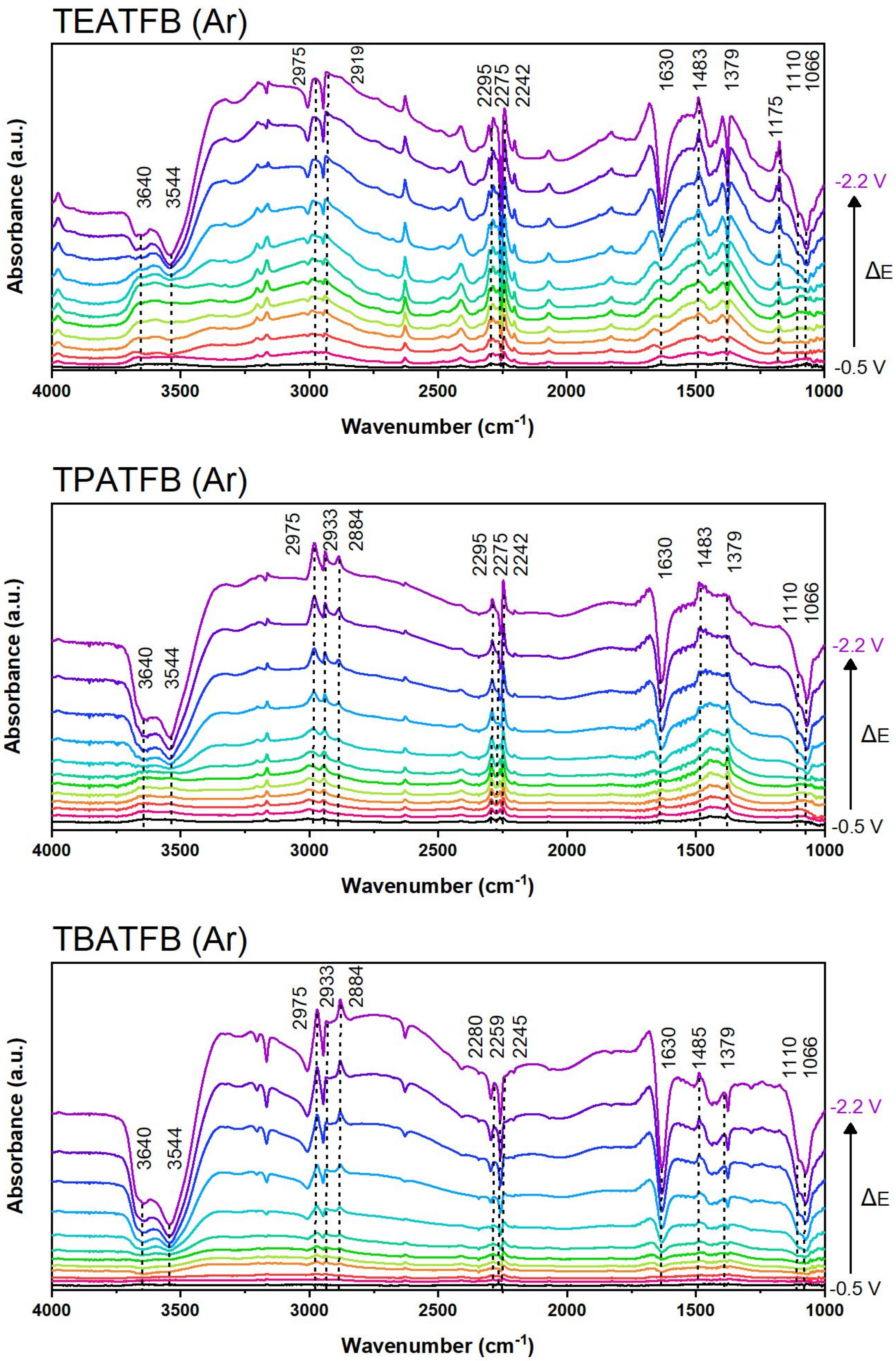


**Figure S13.** Electrochemical in-situ FTIR spectra for wet 0.05 M TEATFB, TPATFB, and TBATFB MeCN electrolytes, in Ar deaerated conditions, at $Cu_{Poly}$ WE. Background signals are recorded at -0.5 V vs $Ag/Ag^{+}$. Spectra are recorded at -0.5 V, then -1.0 V, increasing by -200 mV until -1.4 V, then increasing by -100 mV until -2.2 V.

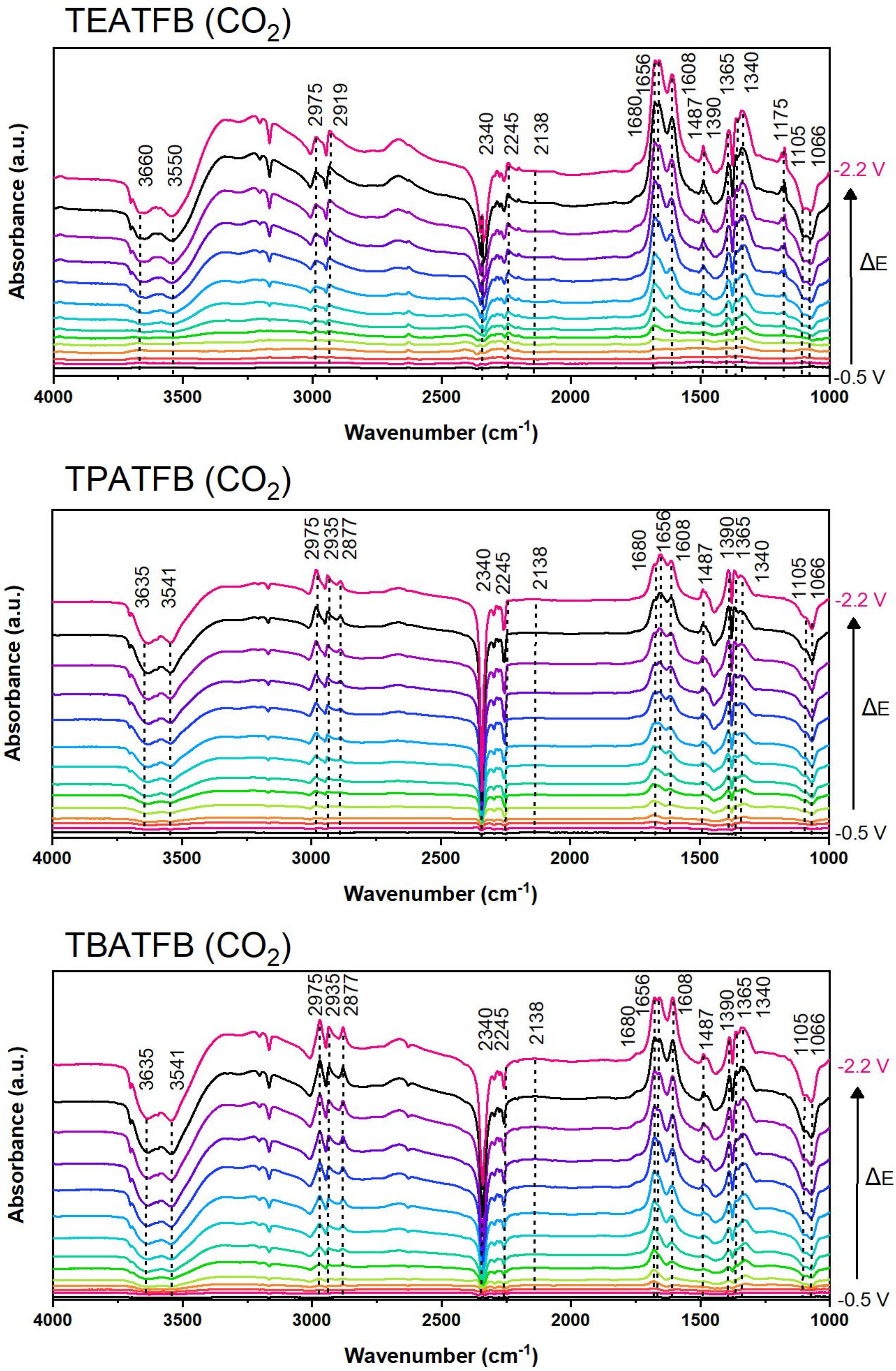


**Figure S14.** Electrochemical in-situ FTIR spectra for wet 0.05 M TEATFB, TPATFB, and TBATFB MeCN electrolytes, in $CO_2$ saturated conditions, at $Cu_{Poly}$ WE. Background signals are recorded at -0.5 V vs Ag/Ag$^+$. Spectra are recorded at -0.5 V, then -1.0 V, increasing by -100 mV until -2.2 V.

**Table S2.** Assignment of the FTIR bands observed in dry and Ar deaerated MeCN electrolytes.

| Wavenumber ($cm^{-1}$) | Assignment | Compound | Reference |
|---|---|---|---|
| 3640 | ν O-H | $H_2O$ | Figueiredo *et. al.*[1] |
| 3544 | ν O-H | $H_2O$ | Figueiredo *et. al.*[1] |
| 2975 | ν C-H | $TAA^+$ | Figueiredo *et. al.*[1] |
| 2919 | ν C-H | $TAA^+$ | Figueiredo *et. al.*[1] |
| 2877 | ν C-H | $TAA^+$ | Figueiredo *et. al.*[1] |
| 2295 | ν C-N | MeCN | Figueiredo *et. al.*[1] |
| 2275 | ν C-N | MeCN | Figueiredo *et. al.*[1] |
| 2245 | ν C-N | MeCN | Figueiredo *et. al.*[1] |
| 2116 | ν C≡N | 3-Aminocrotononitrile | Foley *et. al.*[2] |
| 1690 | ν C=O | $CH_3CONH_2$ | Foley *et. al.*[2] |
| 1650 | ν C=O | $CH_3CONH_2$ | Foley *et. al.*[2] |
| 1520 | ν C=N | 3-Aminocrotononitrile | Foley *et. al.*[2] |
| 1483 | δ $CH_3$ | $CH_3CONH_2$ | Foley *et. al.*[2] |
| 1393 | δ $CH_3$ | $CH_3CONH_2$ | Foley *et. al.*[2] |
| 1175 | δ $NH_2$ | $CH_3CONH_2$ | Foley *et. al.*[2] |
| 1105 | ν $BF_4$ | $BF_4^-$ | Figueiredo *et. al.*[1] |

**Table S3.** Assignment of the FTIR bands observed in dry and $CO_2$ saturated MeCN electrolytes.

| Wavenumber ($cm^{-1}$) | Assignment | Compound | Reference |
|---|---|---|---|
| 3700 | ν O-H | $H_2O$ | Figueiredo *et. al.*[1] |
| 3597 | ν O-H | $H_2O$ | Figueiredo *et. al.*[1] |
| 2975 | ν C-H | $TAA^+$ | Figueiredo *et. al.*[1] |
| 2919 | ν C-H | $TAA^+$ | Figueiredo *et. al.*[1] |
| 2877 | ν C-H | $TAA^+$ | Figueiredo *et. al.*[1] |
| 2340 | ν C=O | $CO_2$ | Figueiredo *et. al.*[1] |
| 2245 | ν C-N | MeCN | Figueiredo *et. al.*[1] |
| 2155 | ν C-O | Cu-*$CO_{(ads)}$ | This work, Moradzaman[3] |
| 2138 | ν C-O | $CO_{(gas)}$ | Figueiredo *et. al.*[1] |
| 1681 | ν C=O | $CO_3^{2-}$ | Figueiredo *et. al.*[1] |
| 1646 | ν C=O | $CO_3^{2-}$ | Figueiredo *et. al.*[1] |
| 1607 | ν C=O | $HCO_3^-$ | Figueiredo *et. al.*[1] |
| 1487 | δ $CH_3$ | $CH_3CONH_2$ | Foley *et. al.*[2] |
| 1390 | ν C-O | $HCO_3^-$ | Figueiredo *et. al.*[1] |
| 1362 | ν C-O | $CO_3^{2-}$ | Figueiredo *et. al.*[1] |
| 1333 | ν C=O | $CO_3^{2-}$ | Figueiredo *et. al.*[1] |
| 1322 | ν C-O | $CO_3^{2-}$ | Figueiredo *et. al.*[1] |
| 1305 | ν C-O | $CO_3^{2-}$ | Figueiredo *et. al.*[1] |
| 1213 | ν C-H | $HCO_3^-$ | Figueiredo *et. al.*[1] |
| 1105 | ν $BF_4$ | $BF_4^-$ | Figueiredo *et. al.*[1] |
| 1066 | ν $BF_4$ | $BF_4^-$ | Figueiredo *et. al.*[1] |

**Table S4.** Assignment of the FTIR bands observed in wet and Ar deaerated MeCN electrolytes.

| Wavenumber ($cm^{-1}$) | Assignment | Compound | Reference |
|---|---|---|---|
| 3640 | ν O-H | $H_2O$ | Figueiredo *et. al.*[1] |
| 3544 | ν O-H | $H_2O$ | Figueiredo *et. al.*[1] |
| 2975 | ν C-H | $TAA^+$ | Figueiredo *et. al.*[1] |
| 2933 | ν C-H | $TAA^+$ | Figueiredo *et. al.*[1] |
| 2884 | ν C-H | $TAA^+$ | Figueiredo *et. al.*[1] |
| 2295 | ν C-N | MeCN | Figueiredo *et. al.*[1] |
| 2275 | ν C-N | MeCN | Figueiredo *et. al.*[1] |
| 2245 | ν C-N | MeCN | Figueiredo *et. al.*[1] |
| 1680 | ν C=O | $CH_3CONH_2$ | Foley *et. al.*[2] |
| 1630 | δ O-H | $H_2O$ | Foley *et. al.*[2] |
| 1483 | δ $CH_3$ | $CH_3CONH_2$ | Foley *et. al.*[2] |
| 1379 | δ $CH_3$ | $CH_3CONH_2$ | Foley *et. al.*[2] |
| 1175 | δ $NH_2$ | $CH_3CONH_2$ | Figueiredo *et. al.*[1] |
| 1110 | ν $BF_4$ | $BF_4^-$ | Figueiredo *et. al.*[1] |
| 1066 | ν $BF_4$ | $BF_4^-$ | Figueiredo *et. al.*[1] |

**Table S5.** Assignment of the FTIR bands observed in wet and $CO_2$ saturated MeCN electrolytes.

| Wavenumber ($cm^{-1}$) | Assignment | Compound | Reference |
|---|---|---|---|
| 3660 | ν O-H | $H_2O$ | Figueiredo *et. al.*[1] |
| 3550 | ν O-H | $H_2O$ | Figueiredo *et. al.*[1] |
| 2975 | ν C-H | $TAA^+$ | Figueiredo *et. al.*[1] |
| 2919 | ν C-H | $TAA^+$ | Figueiredo *et. al.*[1] |
| 2877 | ν C-H | $TAA^+$ | Figueiredo *et. al.*[1] |
| 2340 | ν C=O | $CO_2$ | Figueiredo *et. al.*[1] |
| 2245 | ν C-N | MeCN | Figueiredo *et. al.*[1] |
| 2138 | ν C-O | $CO_{(gas)}$ | Figueiredo *et. al.*[1] |
| 1680 | ν C=O | $CO_3^{2-}$ | Figueiredo *et. al.*[1] |
| 1666 | ν C=O | $CO_3^{2-}$ | Figueiredo *et. al.*[1] |
| 1608 | ν C=O | $HCO_3^-$ | Figueiredo *et. al.*[1] |
| 1487 | δ $CH_3$ | $CH_3CONH_2$ | Foley *et. al.*[2] |
| 1390 | ν C-O | $HCO_3^-$ | Figueiredo *et. al.*[1] |
| 1365 | ν C-O | $CO_3^{2-}$ | Figueiredo *et. al.*[1] |
| 1340 | ν C=O | $CO_3^{2-}$ | Figueiredo *et. al.*[1] |
| 1105 | ν $BF_4$ | $BF_4^-$ | Figueiredo *et. al.*[1] |
| 1066 | ν $BF_4$ | $BF_4^-$ | Figueiredo *et. al.*[1] |

## References


(1) Figueiredo, M. C.; Ledezma-Yanez, I.; Koper, M. T. M. In Situ Spectroscopic Study of $CO_2$ Electroreduction at Copper Electrodes in Acetonitrile. *ACS Catal.* **2016**, *6* (4), 2382–2392.

(2) Foley, J. K.; Korzeniewski, C.; Pons, S. Anodic and Cathodic Reactions in Acetonitrile/Tetra-n-Butylammonium Tetrafluoroborate: An Electrochemical and Infrared Spectroelectrochemical Study. *Can J. Chem.* **2011**, *66*, 201–206.

(3) Moradzaman, M.; Mul, G. Infrared Analysis of Interfacial Phenomena during Electrochemical Reduction of $CO_2$ over Polycrystalline Copper Electrodes. *ACS Catal.* **2020**, *10* (15), 8049–8057.